Comparison of the Electrochemical Behavior of Amorphous $Zr_{55}Cu_{30}Ni_5Al_{10}$, Stainless Steel (316LVM) and CoCrMo (F75) in Simulated Body Fluid with and without Addition of Protein

Ali Tabeshian [a], Dan Persson [b], Lars Arnberg [a, c], Ragnhild E. Aune [a]

[a] Dept. of Material Science and Engineering, Norwegian University of Science and Technology (NTNU), Trondheim, Norway

[b] Dept. of Corrosion and Surface Engineering, Swerea KIMAB AB, Kista, Sweden

[c] Dept. of Material Science and Engineering, Royal Institute of Technology (KTH), Stockholm, Sweden

Abstract

Electrochemical behavior of and metal ion release from the bulk amorphous (glassy) $Zr_{55}Cu_{30}Ni_5Al_{10}$ alloy (Zr-MG) was evaluated at 310 K in simulated body fluid (Phosphate Buffer Saline (PBS)) with and without additions of protein (albumin Fraction V). The passivation behavior and susceptibility to pitting corrosion of the Zr-MG was compared to that of conventional load bearing implant materials, *i.e.* the medical grade ASTM F75 cast CoCrMo alloy (CoCrMo) and AISI 316 LVM low carbon vacuum re-melted Stainless Steel alloy (SS), at pH 7.4 and 5.2. Furthermore, the total metal ion release, as well as the leakage of the main constituent elements of each alloy, were measured and compared. All materials showed passive behavior in the PBS solutions, *i.e.* with and without addition of protein, though the passive region was smaller for the Zr-MG compared to that of the CoCrMo and SS. Moreover, all materials experienced pitting corrosion in pure PBS solution, while the Zr-MG alloy was the most susceptible to pitting and the CoCrMo the least. Additions of protein to the PBS solution prevented the formation of stable pits at both pH 7.4 and 5.2 in the case of the CoCrMo and SS, however, a decrease in the passive region and pitting potential was observed at pH 7.4 for the Zr-MG while the opposite behavior at pH 5.2. Furthermore, the total metal ion release from the Zr-MG was more than for the SS and less than for the CoCrMo.

Keywords: amorphous, CoCrMo, stainless steel, implant, electrochemical measurement, metal ion release.

1. Introduction

Due to the higher life expectancy of humans in general, as well as accidents and sports related injuries, it is predicted that more and more people will need reconstruction/replacement surgeries involving the use of an implant. In the case of load bearing implants, *i.e.* hip and knee implants, the increase in primary implantation surgeries during the time period 2005 to 2030 has in the US been estimated to be 174% and 673% respectively [1]. In this regards it should be mentioned, that the service life time of these implants are presently ~10 to 20 years [2], [3]. The main reason for this is the adverse effect of the aggressive environment of the human body that consist of water, dissolved oxygen and high concentrations of Na^+ and Cl^- ions, along with other electrolytes, *e.g.* bicarbonate and small amounts of potassium, calcium, magnesium, phosphate and sulphate ions, as well as proteins. Furthermore, the pH of the human body can decrease from 7.4 to 5.2 if an infection/inflammation arises in the body, which may occur after implantation of a medical device/implant into the body [4], [5] due to the generation of acidic metabolic products [6]. As a result, these constituents/variables can drastically affect the corrosion and wear properties/behaviors of the material [7]–[9].

Metallic alloys with their combination of high strength, ductility, formability, fracture toughness, wear and corrosion resistance are superior for the use in load bearing implants, where both tensile and bending loads occur [10]. As a result, medical grade CoCrMo alloys and Stainless Steel alloys are conventional biomaterials widely used in these applications today, however, some of their physical, mechanical and chemical properties must be enhanced in order to further improve the

performance of the implant over time and thereby increase its overall service life time. In addition, some of the elements present in these materials, *e.g.* Ni, Cr and Co, are undesirable due to their toxic effect on the human body [11]. It has been reported in literature that Cr (VI) compounds [12] and metallic Ni [13] may be carcinogenic, and Cr [12], Ni [13], and Co [14] are also known to cause allergies. Moreover, these elements also affect the Young´s modulus of both the CoCrMo alloys and Stainless Steel alloys, which may result in a mismatch between the implant and the human bone leading to stress shielding effects [15].

The corrosion behavior of metallic implants is also controlled by the structural and compositional related properties of the oxide film/layer formed on the surface of the implant immediately upon exposer in the human body [6]. The passive oxide film/layer on CoCrMo-based implants consists mainly of Cr-oxide and hydroxide (Cr_2O_3 and $Cr(OH)_3$) with small amounts of Co- and Mo-oxides (Co^{2+}, Co^{3+} and Mo^{4+}) [16], lowering the susceptibility for pitting corrosion [17], [18]. In the case of Stainless Steel alloys, the oxide film/layer consists of two parts, *i.e.* an inner film/layer of Ni-oxide (Ni^{2+} and Ni^{3+}) and an outer of Cr- and Fe-oxides (Cr^{3+} and Fe^{3+}), resulting in a higher corrosion resistivity [19]. However, the Stainless Steel alloys have been reported to be susceptible to pitting corrosion, which obviously has a negative effect on the biocompatibility and mechanical strength of the implant [6]. This can be explained by the adsorption of Cl^- and SO_4^{-2} ions onto the passive film/layer resulting in the pitting corrosion [19].

There are different views on how the human protein affects the corrosion behavior of a metallic implant. Woodman *et al.* [20] found that proteins may enhance the corrosion propagation for some metallic implant materials, and Munoz and Mischler [21] concluded that it limited the adsorption of phosphate to the material surface and thus accelerated the corrosion while simultaneously modifying the passive film properties by acting as a cathodic inhibitor and thereby reducing the

corrosion rate. More or less at the same time, Yan *et al.* [22] reported that proteins increased the corrosion potential and decreased the breakdown potential for both CoCrMo alloys and Stainless steel alloys.

Based on the above, there is obviously a need to optimize the material properties of existing load bearing implant materials, as well as to develop new materials with improved properties. Many researchers have suggested the possible use of composites [23] and polymers [24], as well as Metallic Glasses (MGs) [25]–[33] as potential biomaterials. In regards to MGs, it is the materials overall improved physical, mechanical and chemical properties [31] that have caught researchers attention. As a frozen liquid, MGs fail to crystalize during solidification, resulting in the absence of crystalline defects such as grain boundaries, dislocations and vacancies Zr-based MGs are for example recognized by their high strength (1700 MPa) and hardness (590 HV), as well as relatively low elasticity (50-100 GPa for Zr-based MGs compare to 3-50 GPa for the cortical bone) and corrosion rate [34] [35] [31], [36] in various aqueous environments. However, Zr-based MGs has been reported to be susceptible to pitting corrosion in aqueous solutions containing halide ions (Cl^- and F^-) [37] due to the preferential absorption of Cl^- and F^- ions to the surfaces of the material [38]. In this regard it should be mentioned that the pitting corrosion resistivity of the $Zr_{60}Nb_5Cu_{22.5}Pd_5Al_{7.5}$ and $Zr_{60}Nb_5Cu_{20}Fe_5Al_{10}$ MG alloys has been reported to be better than for most Stainless Steel alloys [26]. The elastic moduli of Zr-based MGs is also close to that of the human bone [15].

The objective of the present work is to clarify the corrosion behavior of, and metal ion release from, the bulk amorphous (glassy) $Zr_{55}Cu_{30}Ni_5Al_{10}$ alloy when exposed in Phosphate Buffer Saline (PBS) solution at pH 7.4 and 5.2, with and without the addition of protein. Various electrochemical techniques, *i.e.* cyclic polarization measurements and electrochemical impedance spectroscopy,

will be used to evaluate the passivation behavior and susceptibility to pitting corrosion. The obtained results will be compared to those of conventional load bearing implant materials, *i.e.* Stainless Steel and CoCrMo.

2. Experimental

2.1 Materials and solutions

The bulk amorphous (glassy) $Zr_{55}Cu_{30}Ni_5Al_{10}$ alloy (Zr-MG) used in the present study was produced at the Advanced Institute for Material Research (AIMR), Tohoku University (Sendai, Japan). Due to the low critical cooling rate needed to produce the material, a one of a kind automatic arc-melter with a water cooled copper mould was used. To confirme the glassy structure of the produced Zr-MG, X-Ray Diffraction (XRD) was used (Bruker D8, Cu/40 kV/150 mA). As can be seen in Figure 1, the XRD pattern does not contain any sharp peaks confirming the lack of crystals in the structure. However, diffuse peaks at $2\theta = 38°$ and 65° were identified, which is in accordance with previously reported patterns for similar Zr-based MGs [5].

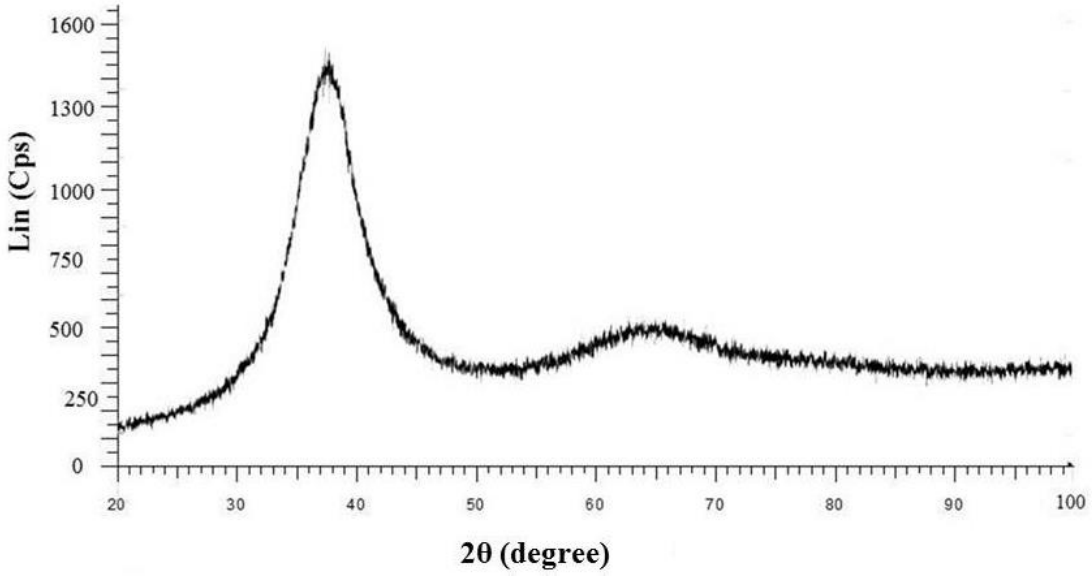

Figure 1. XRD pattern for the Zr-MG sample indicating the glassy structure.

Moreover, medical grade ASTM F75 cast CoCrMo alloy (CoCrMo) and AISI 316 LVM low carbon vacuum re-melted Stainless Steel alloy (SS) were used for the comparison. The chemical compositions and the geometric shape of all materials are presented in Table 1.

Table 1. Chemical composition and geometric shape of the Zr-MG, CoCrMo and SS alloys.

Materials	**Type**	**Shape**	**Chemical composition (wt%)**								
			Fe	Co	Zr	Cr	Ni	Mo	Mn	Cu	Al
SS	AISI 316LVM	rod	62.59			16.52	14.50	4.74	1.65		
CoCrMo	ASTM F75	rod		66.64		2.16	0.19	8.02			
Zr-MG	$Zr_{55}Cu_{30}Ni_5Al_{10}$	droplet			67.01		3.92			25.46	3.60

The initial preparation of all samples consisted of cutting the materials into 5 mm thick discs, grinding and polishing to a mirror-like surface (4000 #SiC) to remove any oxide film/layer and/or reduce surface defects, cleaning in an ultrasonic ethanol bath for 2 minutes, and drying in warm air.

Two artificial body fluids (PBS) were prepared, *i.e.* with and without the additions of protein (albumin Fraction V, also known as Bovine Serum Albumin (BSA)). A mixture of 42.4 mM K_2HPO_4 (MERCK 99%), 7.6 mM KH_2PO_4 (MERCK 99%) and 0.15 M NaCl (MERCK 99%) diluted with distilled water was used for the preparation of the PBS solution at a concentration of 0.05 M. For the PBS solution with additions of protein, the albumin Fraction V (MERCK 99%) was added at a concentration of 2 g/L, which was the maximum amount needed to reach a saturated monolayer of protein on the surface of all materials [39] (from here on albumin Fraction V will be referred to as albumin).

2.2 Electrochemical measurements

The electrochemical measurements were carried out with the PBS solution, with and without additions of albumin, as the electrolyte. All experiments were performed at body temperature and at two different pH levels (7.4 and 5.2). The electrochemical cell used consisted of a Working Electrode (WE) exposing an area of 0.18 cm^2 to the electrolyte, a platinum Counter Electrode (CE), and a Saturated Calomel Electrode (SCE) (+ 0.2444 V vs. Standard Hydrogen Electrode, Radiometer analytical - Ref 401). Water at 310 K (37 °C) was circulated around the cell to secure a constant temperature throughout the experiment. Furthermore, a Solartron Mobery potentiostat with an acquisition rate of 5 points/sec and a scanning rate of 2 mV/sec was used to vary the potential of the sample. The measurements were controlled through the CorrWare® Software (Windows version 3.9).

The basic cell configuration was first used to perform the Open Circuit Potential (OCP) measurements to assure the formation of an oxide film/layer on the surface of the sample. The experiment was performed for 1 hour to secure stable conditions between the electrolyte and the sample. The cyclic polarization test was a direct continuation of the OCP measurement. The sample was polarized in the cathodic direction (negative) to -1.5 V vs. SCE to remove any contamination on the surface of the sample, and to secure the formation of a uniform oxide-free film/layer. Further, the sample was polarized in the anodic direction (positive) to 0.6 V vs SCE for the Zr-MG sample and 1.5 V for the SS and CoCrMo samples to again form an oxide film/layer on the surface of the samples. The maximum potential in the case of the Zr-MG sample was less due to the breakage of the oxide film/layer at a higher voltage. In the final step of the cyclic polarization test, the sample was again polarized in the cathodic direction to -1.5 V vs. SCE.

In the case of the Electrochemical Impedance Spectroscopy (EIS) measurement, the same electrochemical cell as for the cyclic polarization test was used. However, for these measurements, an Autolab PGSTAT 302 potentiostat connected to a frequency response analyzer, module FRA2 (Eco Chemie B.V.), were used. The amplitude of the sinusoidal AC perturbation applied to the sample was 10 mV. Even in this case, the measurements were performed at the OCP after stabilization for 1 h.

2.3 Immersion test

To evaluate the metal ion release from the samples into the electrolyte, an immersion test was carried out in accordance with the EN ISO 10993-15 standard (*Biological Evaluation of Medical Devices — Part 15: Identification and Quantification of Degradation Products from Metals and Alloys*) [40]. Samples with a mirror-like surface finish (4000 #SiC) were exposed to the PBS solution with additions of albumin for one week at 310 K. During the immersion tests, the samples were slowly shaken at a frequency of 15 RPM to secure the homogeneity of the electrolyte throughout the test. The produced degradation products were analyzed using an Inductively Coupled Plasma Mass Spectroscopy (ICP-MS) unit (Thermo Scientific XSERIES 2 ICP-MS), operated with Xt interface cones, a quartz concentric nebulizer, impact bead Peltier cooled spray chamber, and a standard 1.5 mm in diameter injector single piece quartz torch.

3. Results and discussion

3.1 Electrochemical behavior

The results from the cyclic polarization test performed in the pure PBS solution have been plotted as current density (I) vs. potential (E) in Figure 2 (a)-(c) for the Zr-MG, CoCrMo and SS samples. As can be seen form the figure, four well-defined domains can be identified for all samples, *i.e.*:

1. The cathodic domain below the E_{corr} where the reduction of oxides and removal of contaminants from the sample surface are taking place.
2. At the E_{corr} where the transition from cathodic to anodic potentials is taking place.
3. The anodic domain above the E_{corr} where the current remains stable over a range of electrode potentials (E) forming a passive plateau.
4. The transpassive domain where an abrupt increase in the current is obtained.

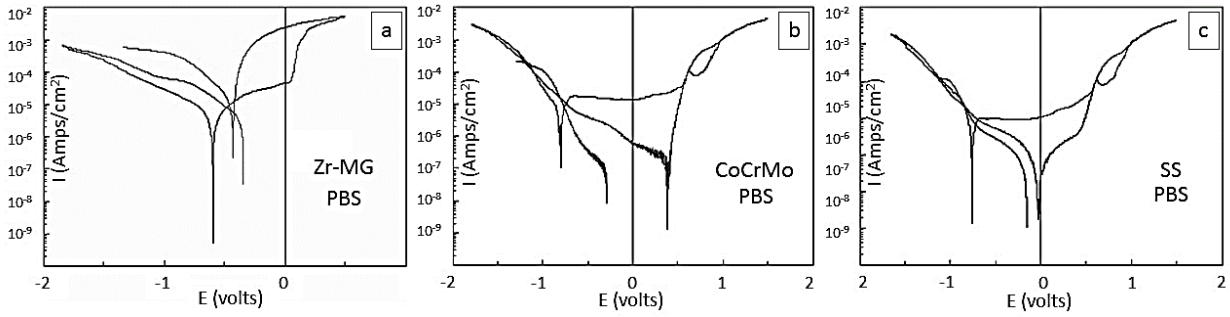

Figure 2. Cyclic polarization plots of the current density (I) vs. potential (E) in pure PBS solution for (a) Zr-MG, (b) CoCrMo, and (c) SS samples. Overall experimental conditions: 310 K and pH 7.4.

As can be seen from Figure 2 (a), the Zr-MG sample has a passive region at approximately - 0.5 to 0.1 V, followed by an abrupt increase in the current, as well as a large hysteresis loop clearly indicating a susceptibility to pitting corrosion. In the case of both the CoCrMo and SS samples, a passive region can be seen in Figure 2 (b) and (c) at approximately - 0.7 to 0.5 V followed by an oxidation peak at approximately 0.6 V. The peak is the result of the oxidation of Cr^{3+} ions to Cr^{6+} ions which occurs due to the presence of phosphate ions in the electrolyte. The larger passive

region obtained for the CoCrMo and SS samples, as well as the smaller hysteresis loop, confirms a higher corrosion resistivity and lower tendency of pitting corrosion for these materials.

Repassivation behavior was obtained for all samples during the backward scan. As can be seen form Figure 2 (a)-(c), the curves passes through the passivation region and the damaged passive layer is to some extend recovered, which is in agreement with previously reported results [6], [21], [41].

3.1.1 pH effect

In Figure 3 (a)-(c) the results from the polarization test performed in pure PBS solution at pH 5.2 have been plotted together with the previously obtained results for pH 7.4. The figure shows the current density (I) vs. potential (E) for the Zr-MG, CoCrMo and SS samples. As can be seen in Figure 3 (a), the passive region of the Zr-MG sample clearly decreases when the pH is lowered from 7.4 to 5.2, and as a result the pitting occurs at a lower potential. In other words, decreasing the pH level accelerates the dissolution of the oxide film/layer on the surface of the sample. Furthermore, due to the increased proton concentration in the electrolyte the cathodic reaction is also accelerated resulting in a decrease of the pitting potential.

As can be seen from Figure 3 (b) and (c), decreasing the pH level has little effect on the width of the passive region in the case of the CoCrMo and SS samples. Similar effect was also identified for the crystalline $Zr_{55}Cu_{30}Ni_5Al_{10}$, which showed minor change in its electrochemical behavior by lowering the pH level [42]. Moreover, the Cr^{3+} oxidation peak for the CoCrMo and SS samples has disappeared, and a pronounced activation peak can be seen at - 0.6 V for the CoCrMo sample.

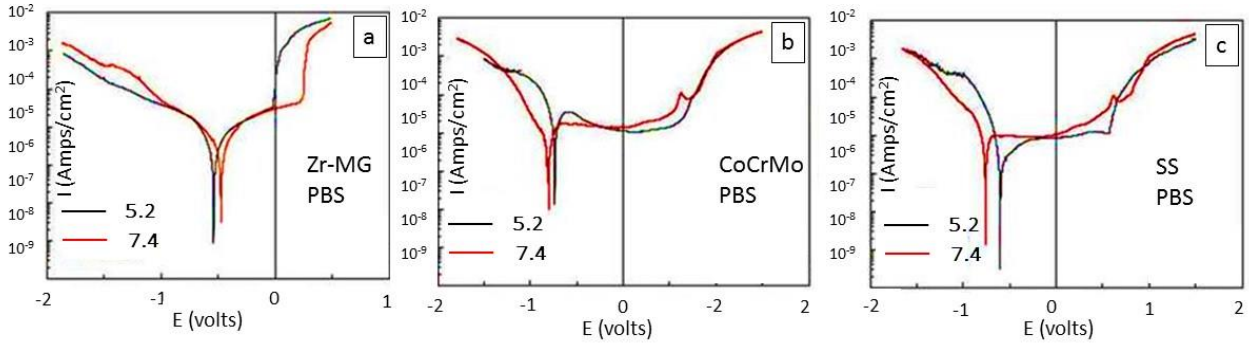

Figure 3. Polarization curves in pure PBS solutions for (a) Zr-MG, (b) CoCrMo, and (c) SS samples. Overall experimental conditions: 310 K and pH 7.4 and 5.2.

3.1.2 Protein effect

In Figure 4 (a)-(b) the effect of protein (albumin) on the cyclic polarization curve of the Zr-MG sample is plotted for pH 7.4 and 5.2, and compared to the previously obtained results in pure PBS solution. As can be seen from Figure 4 (a), a small decrease of the passive region and a lowering of the pitting potential were obtained at pH 7.4, while the opposite was obtained at pH 5.2, see Figure 4 (b). It is believed that this effect is related to the difference in the charge of the albumin molecules, which decreases as it gets closer to its isoelectric point at pH 4.7-4.9. Due to the reduction of the charge of the albumin, the amount of electrostatic repulsive forces between the albumin molecules will decrease as an increasing amount of albumin attaches to the surface of the sample creating a more closely-packed adsorption layer. Moreover, the destabilization of the passive film in the presence of albumin can be related to the formation of metal-protein complexes.

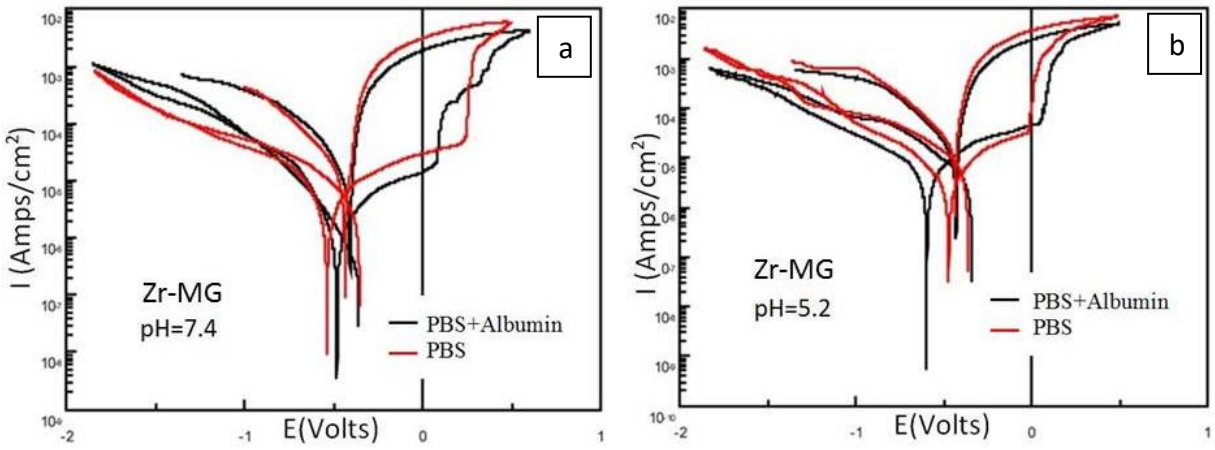

Figure 4. Cyclic polarization curves in PBS solution with and without additions of albumin for the Zr-MG sample. Overall experimental conditions: 310 K, pH 7.4 and pH 5.2, as well as additions of 2 g/L albumin.

The same figures were also plotted for the CoCrMo and SS samples, Figure 5 (a)-(b) and Figure 6 (a)-(b) respectively. As can be seen in Figure 5 (a)-(b), the addition of albumin effects the repassivation and pitting behaviors of the CoCrMo sample both at pH 7.4 and pH 5.2. The disappearance of the hysteresis from the cyclic polarization curve indicates that the albumin inhibits the formation of stable pits by the adsorption of protein molecules to the initiation sites for the pits and thereby improving the corrosion resistivity. In the case of pH 7.4, similar results are also obtained for the SS sample, see Figure 6 (a). However, in pure PBS solution at pH 5.2 the cyclic polarization curve shows typical pitting and repassivation behavior.

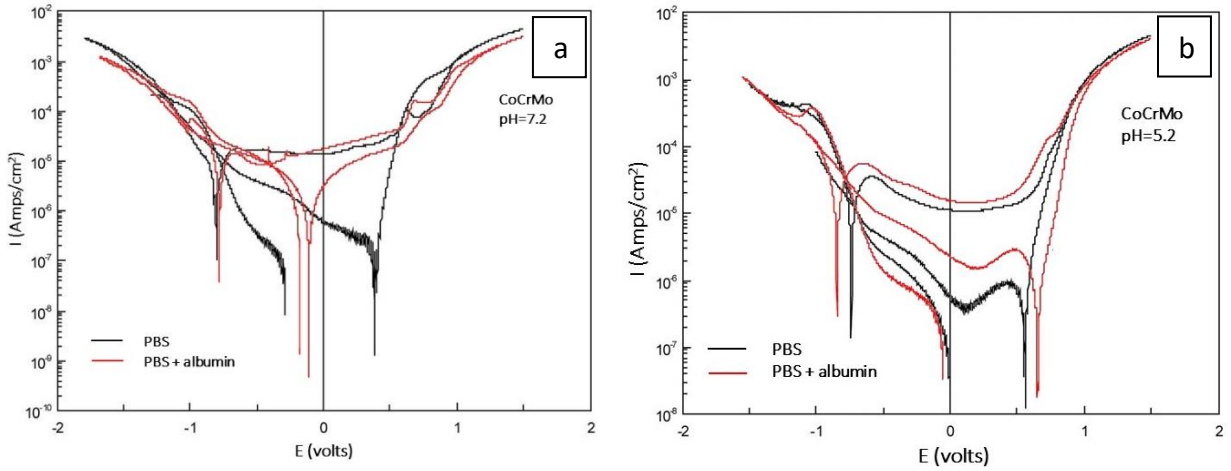

Figure 5. Cyclic polarization curves in PBS solution with and without additions of albumin for the CoCrMo sample. Overall experimental conditions: 310 K, pH 7.4 and pH 5.2, as well as additions of 2 g/L albumin.

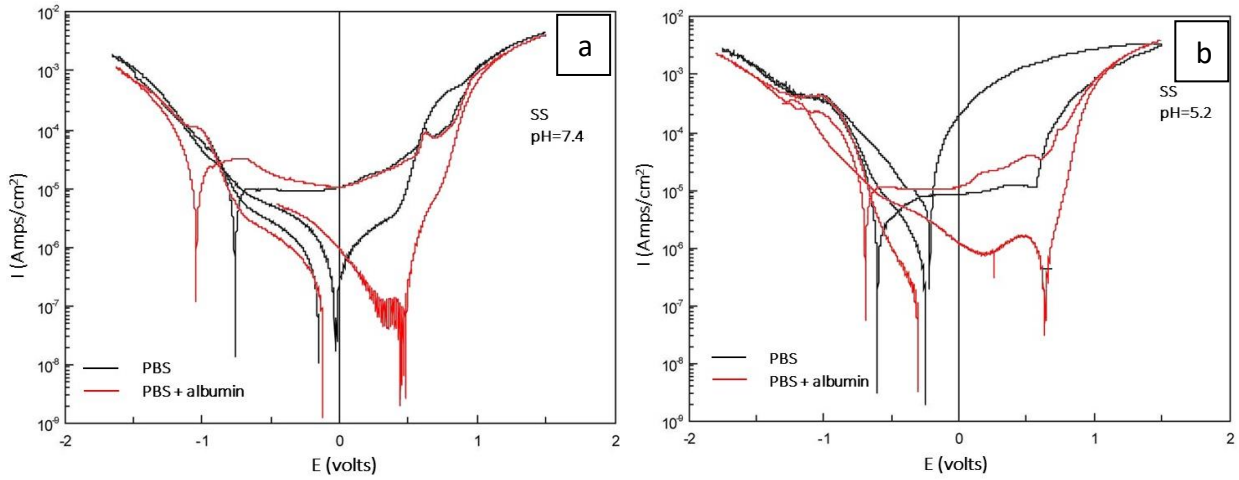

Figure 6. Cyclic polarization curves in PBS solution with and without additions of albumin for the SS sample. Overall experimental conditions: 310 K, pH 7.4 and pH 5.2, as well as additions of 2 g/L albumin.

3.1.2 Electrochemical Impedance Spectroscopy (EIS)

The EIS measurements were performed in PBS solution with and without additions of protein at pH 7.4. In Figure 7 (a) and (c), the Nyquist diagrams for the Zr-MG, CoCrMo and SS samples are plotted as the real part of the recorded impedance at one frequency (Z′) vs. the imaginary part (Z″).

As can be seen from the figures, a large transition resistance is obtained between the electrode and the electrolyte for all samples in both cases. The grater size of the depressed semi-circle for the CoCrMo sample compared to those of the Zr-MG and SS samples reveals the materials higher degree of corrosion resistivity due to the presence of a more stable oxide film/layer on the surface in this case.

In Figure 7 (b) and (d), the Bode diagrams for the Zr-MG, CoCrMo and SS samples are plotted. The Bode diagram consists of two plots that show how the amplitude ratio (|Z|) and phase angle (theta) vary with frequency. As can be seen from the figures with the phase angle, the Zr-MG samples show the same behavior in both electrolytes, *i.e.* two time-constants are obtained. The first time-constant is at a lower frequency and represents the interface between the film/layer and the electrolyte indicating the onset of the corrosion process. The second time-constant, which is at a higher frequency and with a more pronounced shape, indicates the presence of an oxide film/layer on the surface of the material. When comparing the two time-constants between the measurements performed in pure PBS solution and in the PBS solution with additions of albumin, the first and second time-constants are both at higher frequencies when the sample is exposed in pure PBS solution indicating the better corrosion resistivity obtained in this case. This is further confirmed by the higher phase anglr obtained for the first time-constant in the pure PBS solution, *i.e.* -75° and -62° respectively.

In the case of the CoCrMo and SS samples the albumin has minor effect on the spectra compared to the Zr-MG sample. Furthermore, the linear portion of the spectra at intermediate frequencies indicates the presence of a compact passive film/layer on the surface of these materials, which is in agreement with previously reported results [21] , [43], [44].

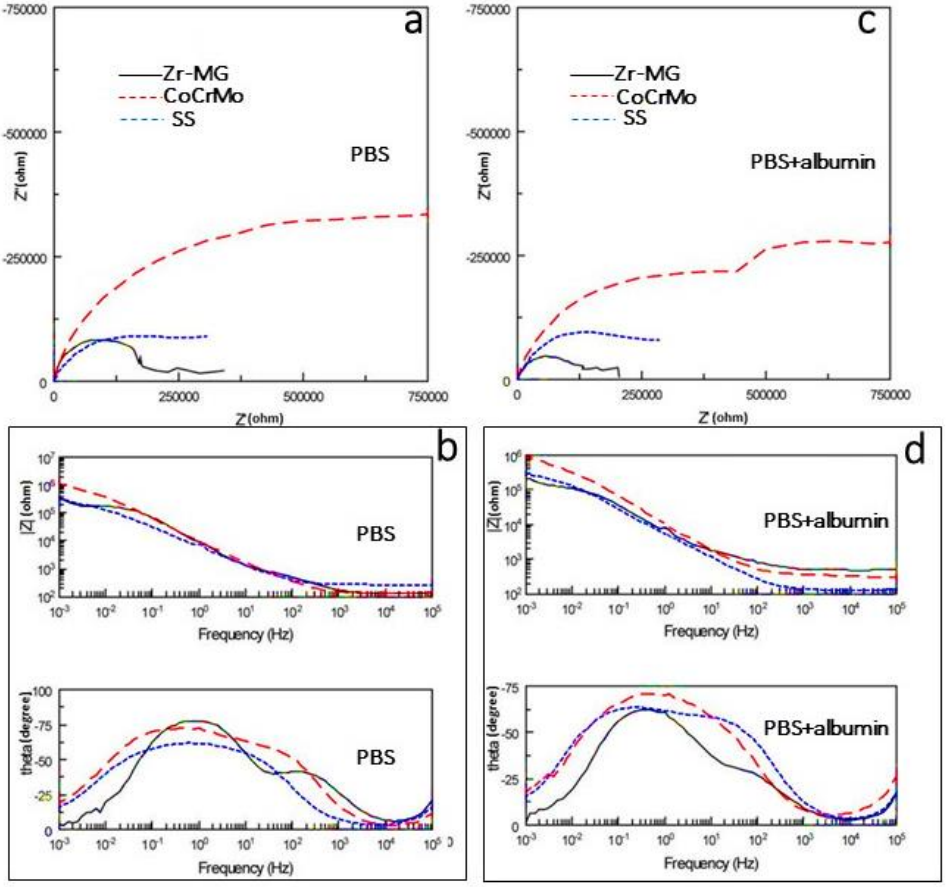

Figure 7. Impedance measurements after holding the samples at the OCP for 1 h in pure PBS. (a) Nyquist plots and (b) Bode plots, based on EIS measurements performed in pure PBS solution, and (c) Nyquist plots and (d) Bode plots, based on EIS measurements performed in PBS solution with additions of 2 g/L albumin. Overall experimental conditions: 310 K and pH 7.4.

3.2 Metal ion release measurements

The total metal ion release from all samples (Zr-MG, CoCrMo and SS) was measured after 1-week of exposure in PBS solution with additions of albumin (2 g/L at pH 7.4 and 310 K). The Ni-ion release was given special attention, as it is considered to be toxic to the human body and the only element present in all samples.

In Table 2 the total metal ion release from each sample is presented, as well as the amount released of each of the major elements present in each sample. As can be seen from the table the CoCrMo sample has the highest release of metal ions with 0.617 µg/day·cm^2, which is mainly due to the release of Co-ions (0.5758 µg/day·cm^2), while the SS sample has the lowest with 0.051 µg/day·cm^2 which is mainly due to the release of Fe-ions (0.0343 µg/day·cm^2) and Ni-ions (0.01408 µg/day·cm^2). In the case of Cr-ions, which is present in the oxide film/layer of both the CoCrMo and SS samples, the release is low (0.02175 and 0.00079 µg/day·cm^2 respectively). This clearly confirms the stronger bonding of the Cr-ions in the morphological structure of the oxide film/layer on the surface of these samples, results in the higher stability in view of metal ion release. The total metal ion release from the Zr-MG sample was 0.197 µg/day·cm^2, which is mainly due to the release of the Cu-ions enriched in the oxide film/layer present on the surface of the sample as a result of selective oxidation of Cu during the electrolytic process (0.1118 µg/day·cm^2).

Table 2. Total metal ion release from the Zr-MG, CoCrMo and SS samples after 1-week of exposer in a PBS solution with additions of albumin, as well as the amount released of each of the major elements present in each sample. Overall experimental conditions: 310 K and pH 7.4.

Material	**µg/day·cm^2**									
	Al	**Cr**	**Mn**	**Fe**	**Co**	**Ni**	**Cu**	**Zr**	**Mo**	**Total**
Zr-MG	0.0288					0.0078	0.1118	0.0482		0.1966
CoCrMo		0.0218			0.5758	0.0036			0.0164	0.6176
SS		0.0008	0.0006	0.0343		0.0141			0.0007	0.0505

In Figure 8 (a)-(b) the release of Ni-ions from each of the materials is presented in µg/day·cm^2 and in % of the initial Ni concentration. As can be seen from the figure, the release in µg/day·cm^2 is highest from the SS sample (0.0141 µg/day·cm^2); however, with an initial Ni concentration of

14.50 wt% this amounts to a release of only 0.097 % of the Ni. This is believed to be due to the stronger bonding of Ni in the morphological structure of the SS sample. It can also be seen from the figure that the release in µg/day·cm^2 is lowest from the CoCrMo sample (0.0036 µg/day·cm^2), which with an initial Ni concentration of 0.19 wt%, amounts to the highest release of Ni measured in the present study (1.895 %). In the case of the Zr-MG sample, which initially had a Ni concentration of 3.92 wt%, the numbers measured are 0.0078 µg/day·cm^2 and 0.199% respectively. The release of Ni from the Zr-MG sample is more consistent with its initial bulk concentration and results even in this case from the stronger bonding of Ni in the morphological structure of the sample.

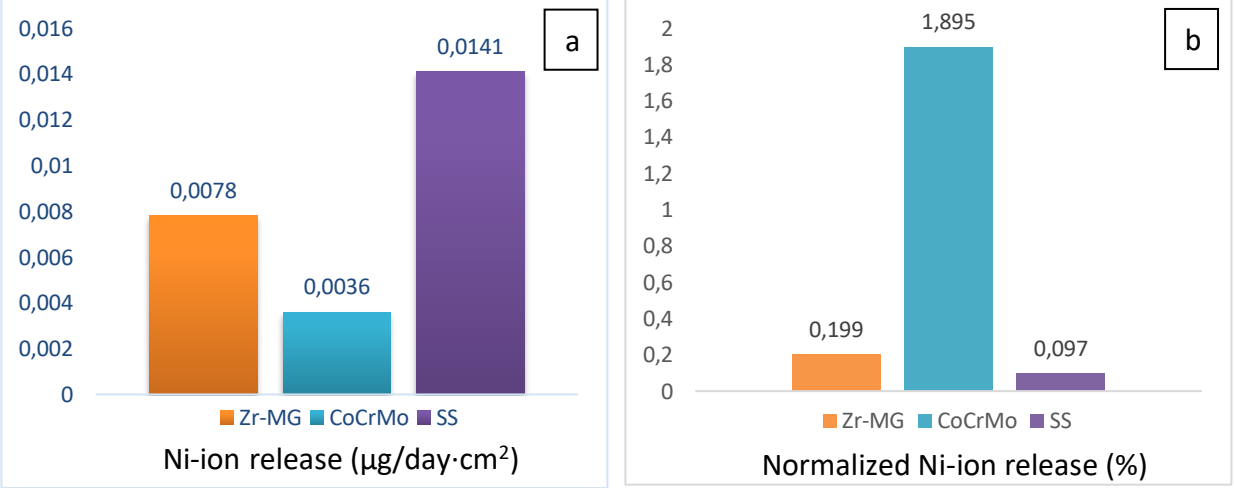

Figure 8. The Ni-ion release from the Zr-MG, CoCrMo and SS samples after 1-week of exposer in a PBS solution with additions of albumin. (a) µg/day·cm^2 and (b) % of the initial Ni concentration. Overall experimental conditions: 310 K and pH 7.4.

4. Conclusions

The passivation behavior and corrosion properties of the bulk amorphous (glassy) $Zr_{55}Cu_{30}Ni_5Al_{10}$ alloy (Zr-MG) in PBS solution with and without additions of albumin, as well as the metal ion

release from the alloy, were studied. Furthermore, the obtained results were compared to that of conventional load bearing implant materials, *i.e.* the medical grade ASTM F75 cast CoCrMo alloy (CoCrMo) and the AISI 316 LVM low carbon vacuum re-melted Stainless Steel alloy (SS).

The Zr-MG proved to have a smaller passive region and lower pitting corrosion potential than the conventional implant materials CoCrMo and SS. Furthermore, albumin additions decreased the passive region as well as the pitting potential at pH 7.4, while the opposite behavior was confirmed at pH 5.2. In the case of CoCrMo and SS, albumin additions hindered the formation of stable pits at both pH 7.4 and pH 5.2. Moreover, the Zr-MG proved to have a lower leakage of metal ions than CoCrMo, but higher than SS.

Based on the presently obtained results it was concluded that the Zr-MG alloy investigated is not suited for the use as an implant material, due to its increased susceptibility to pitting corrosion. However, the positive effect of albumin additions on the corrosion resistivity at pH 5.2, as well as its structural stability in regards to metal ion release, are desirable properties that make Zr-based MG alloys interesting candidates for further investigation.

Acknowledgement

The authors would like to thank Dr. Yoshihiko Yokoyama and the Advanced Institute for Materials Research (AIMR) at Tohoku University, Japan, for providing the $Zr_{55}Cu_{30}Ni_5Al_{10}$ samples, as well as the Norwegian University of Science and Technology (NTNU), Faculty of Natural Sciences and Technology through the Strategic Area Materials, for financial support.

References

[1] S. Kurtz, K. Ong, E. Lau, F. Mowat, M. Halpern, *JBJS*, **2007**, *89*, 780.

[2] “http://hipknee.aahks.net/total-hip-replacement/”, **2017** .

[3] M. Geetha, A. K. Singh, R. Asokamani, A. K. Gogia, *Prog. Mater. Sci.*, **2009**, *54*, 397.

[4] S. Hiromoto, A. Tsai, M. Sumita, T. Hanawa, *Corrosion*, **2000**, *42*, 2193.

[5] Y. Yokoyama, E. Mund, A. Inoue, L. Schultz, *J. Phys. Conf. Ser.*, **2009**, *144*, 12043.

[6] A. Shahryari, S. Omanovic, J. a. Szpunar, *Mater. Sci. Eng. C*, **2008**, *28*, 94.

[7] S. Mischler, A. I. Muñoz, *Wear*, **2013**, *297*, 1081.

[8] K. Prasad, O. Bazaka, M. Chua, M. Rochford, L. Fedrick, J. Spoor, R. Symes, M. Tieppo, C. Collins, A. Cao, D. Markwell, K. Ostrikov, K. Bazaka, *Materials (Basel)*, **2017**, *10*, 884.

[9] D. C. Hansen, *Electrochem. Soc. Interface*, **2008**, *17*, 31.

[10] N. Hallab, J. J. Jacobs, J. Katz, *Biomaterials Science, An Introduction to Materials in Medicine*, 2nd ed. Amsterdam: Elsevier Academic Press, **2004**.

[11] J. T. Minang, I. Areström, M. Troye-Blomberg, L. Lundeberg, N. Ahlborg, *Clin. Exp. Immunol.*, **2006**, *146*, 417.

[12] S. Wilburg, H. Abadin, M. Fay, D. Yu, L. Ingerman, *Public Health*, **2000**, p. 421.

[13] M. Fay, S. Wilbur, and H. Abadin, *U.S Public Heal. Serv. Agency Toxic Subst. Dis. Regist.*, **2005**, p. 397.

[14] O. M. Faroon, H. Abadin, S. Keith, M. Osier, L. Chappell, G. Diamond, G. Sage, *Agency Toxic Subst. Dis. Regist.*, **2004**, p. 486.

[15] D. R. Sumner, *J. Biomech.*, **2015**, *48*, 797.

[16] A. W. E. Hodgson, S. Kurz, S. Virtanen, V. Fervel, C.-O. A. Olsson, S. Mischler, *Electrochim. Acta*, **2004**, *49*, 2167.

[17] H. J. Mueller, E. H. Greener, *J. Biomed. Mater. Res.*, **1970**, *4*, 29.

[18] B. Syrett, *The Application of Electrochemical Techniques to the Study of Homogeneous Chemical Reactions*. Texas: NACE Int, **1977**.

[19] C.-O. Olsson, D. Landolt, *Electrochim. Acta*, **2003**, *48*, 1093.

[20] J. L. Woodman, J. Black, S. A. Jiminez, *J. Biomed. Mater. Res.*, **1984**, *18*, 99.

[21] A. I. Muñoz, S. Mischler, *J. Electrochem. Soc.*, **2007**, *154*, 562.

[22] Y. Yan, A. Neville, and D. Dowson, *Tribol. Int.*, **2007**, *40*, 1492.

[23] H. Oliveira, S. Catros, O. Castano, S. Rey, R. Siadous, D. Clift, J. Marti-Munoz, M. Batista, R. Bareille, J. Planell, E. Engel, J. Amédée, *Acta Biomater.*, **2017**, *54*, 377.

[24] S. Strandman, X. X. Zhu, in *Woodhead Publishing Series in Biomaterials*, Woodhead Publishing, **2015**, pp. 219–245.

[25] Y. Liu, Y.-M. Wang, H.-F. Pang, Q. Zhao, L. Liu, *Acta Biomater.*, **2013**, *9*, 7043.

[26] Q. Chen, L. Liu, S.-M. Zhang, *Front. Mater. Sci. China*, **2010**, *4*, 34.

[27] N. Hua, L. Huang, W. Chen, W. He, T. Zhang, *Mater. Sci. Eng. C*, **2014**, *44*, 400.

[28] S. L. Zhu, X. M. Wang, F. X. Qin., A. Inoue, *Mater. Sci. Eng. A*, **2007**, *459*, 233.

[29] J. Oak, *J. Mater.*, **2007**, *22*, 2.

[30] S. L. Zhu, X. M. Wang, F. X. Qin, M. Yoshimura, A. Inoue, *Mater. Trans.*, **2007**, *48*, 2445.

[31] M. Demetriou, A. Wiest, D. Hofmann, W. Johnson, B. Han, N. Wolfson, G. Wang, P. Liaw, *JOM*, **2010**, *62*, 83.

[32] S. L. Woo, W. H. Akeson, R. D. Coutts, L. Rutherford, D. Doty, G. F. Jemmott, D. Amiel, *J. Bone & Jt. Surg.*, **1976**, *58*, 190.

[33] Y. S. Sun, W. Zhang, W. Kai, P. K. Liaw, H. H. Huang, *J. Alloys Compd.*, **2014**, *586*, 1.

[34] G. Liu, F. Wang, Y. Cao, Y. Sun, *Mater. Trans.*, **2015**, *56*, 1925.

[35] A. L. Greer, *Mater. Today*, **2009**, *12*, 14.

[36] M. L. Morrison, R. A. Buchanan, R. V Leon, C. T. Liu, B. A. Green, P. K. Liaw, J. A. Horton, *Wiley Intersci.*, **2005**, *74*, 430.

[37] J. R. Scully, A. Gebert, J. H. Payer, *J. Mater. Res.*, **2007**, *22*, 302.

[38] C. Suryanarayana, A. Inoue, *Bulk Metallic Glasses*, CRC Press, **2009**.

[39] A. Tabeshian, *MSc. Thesis*, NTNU, Trondheim, Norway, **2011**.

[40] "EN ISO 10993-15, Biological evaluation of medical devices - part 15: Identification and quantification of degredation products from metals and alloys."

[41] A. Gebert, K. Buchholz, A. Leonhard, K. Mummert, J. Eckert, L. Schultz, *Mater. Sci. Eng. A*, **1999**, *267*, 294.

[42] A. Tabeshian, D. Persson, L. Arnberg, R. E. Aune, *Mater. Corros.*, **2016**, *67*, 748.

[43] D. Mareci, D. Sutiman, A. Cailean, G. Bolat, *Prot. Met. Phys. Chem. Surfaces*, **2011**, *47*, 108.

[44] M. J. K. Lodhi, K. M. Deen, Z. U. Rahman, A. Farooq, W. Haider, *J. Ind. Eng. Chem.*, **2018**.